Active and passive sensing of collective atomic coherence in a superradiant laser

Justin G. Bohnet,* Zilong Chen, Joshua M. Weiner, Kevin C. Cox, and James K. Thompson
JILA, NIST, and Department of Physics, University of Colorado, Boulder, Colorado 80309-0440, USA
(Received 8 August 2012; revised manuscript received 24 January 2013; published 17 July 2013)

We study the nondemolition mapping of collective quantum coherence onto a cavity light field in a superradiant, cold-atom ^{87}Rb Raman laser. We show theoretically that the fundamental precision of the mapping is near the standard quantum limit on phase estimation for a coherent spin state, $\Delta\phi = 1/\sqrt{N}$, where N is the number of atoms. The associated characteristic measurement time scale $\tau_W \propto 1/N$ is collectively enhanced. The nondemolition nature of the measurement is characterized by only 0.5 photon recoils deposited per atom due to optical repumping in a time τ_W. We experimentally realize conditional Ramsey spectroscopy in our superradiant Raman laser, compare the results to the predicted precision, and study the mapping in the presence of decoherence, far from the steady-state conditions previously considered. Finally, we demonstrate a hybrid mode of operation in which the laser is repeatedly toggled between active and passive sensing.

DOI: 10.1103/PhysRevA.88.013826 PACS number(s): 42.55.Ye, 32.80.Qk, 37.30.+i, 42.50.Lc

I. INTRODUCTION

Superradiant lasers have the potential to be the most stable optical frequency references to date, with broad impacts across science and technology [1,2]. These frequency references derive their stability from an ensemble of atoms spontaneously synchronized by cavity-mediated interactions, achieving collective coherence times greater than single-particle coherence times [3]. Reliance on interparticle interactions makes superradiant lasing one of the growing number of examples of collective phenomena being explored for enhancing precision measurements [4–11].

The superradiant laser's defining feature is the storage of the coherence of the laser system in the gain medium. The coherence is mapped onto the cavity field through superradiant emission [Fig. 1(a)]. This conceptual Bloch sphere [12] model of the laser has been the key to understanding not only the laser spectrum [3], but also the output field stability properties [13] and ability to use the laser as a sensor of magnetic fields [14]. In a Raman laser configuration, the mapping can be dynamically controlled through the use of an externally applied dressing laser. The storage and recovery of phase information in the atomic ensemble is analogous to quantum memories for quantum communication [15–20].

In this paper, we present an analysis of the nondemolition mapping of the coherence in a self-synchronized ensemble of atoms onto a cavity field through superradiant emission that relies on fundamentally collective effects with no single-atom analog. We link the well-known Schawlow-Townes laser linewidth limit [21] to the information gained about the atomic system through the mapping, which sets the fundamental limit to potential superradiant sensors, and study spontaneous synchronization in the presence of decoherence far from steady-state conditions. Theoretically, the output light provides sufficient information to continuously track the evolving phase of the atomic coherence ϕ with a precision within a factor of 2 of the standard quantum limit (SQL) on phase resolution for a coherent spin state. The coherence readout rate is collectively enhanced by a factor of N compared to single-particle fluorescence readout. Each measurement also prepares the coherence for the next measurement, while only imparting $1/2$ photon recoils per atom in the characteristic measurement time.

Our theoretical analysis is compared to experimental data from our proof-of-principle experimental system using ^{87}Rb [Figs. 1(b) and 1(c)] [3]. The results culminate in a hybrid sensor that combines active sensing of the collective atomic phase during superradiant emission with passive phase measurements using Ramsey-like evolution times. We show the sensor can repeat many measurement cycles in a single experimental trial due to the nondemolition nature of the superradiant mapping.

II. THEORY OF THE OPTIMAL ESTIMATOR

Our theory considers an ideal cold-atom Raman laser. Examples of cold-atom Raman lasers include Refs. [22–25]. The ideal laser we consider here operates deep into the bad-cavity, or superradiant, regime [26,27], where the cavity power decay rate κ greatly exceeds all other relevant decay and scattering rates. The laser utilizes N atoms trapped in a one-dimensional (1D) optical lattice that is formed inside the optical cavity that also mediates the long-range interactions between atoms that drive spontaneous synchronization of the atomic dipoles.

The optical Raman dressing laser induces a decay rate γ from $|\uparrow\rangle$ to $|\downarrow\rangle$ [Fig. 1(c)]. The dressing laser is detuned from an optically excited intermediate state $|i\rangle$, and the rate a single atom scatters photons from the dressing laser into the resonant cavity mode is $\Gamma_c = C\gamma$, where C is the single-particle cavity cooperativity parameter of cavity quantum electrodynamics (QED) [28]. The collective cooperativity satisfies the necessary condition for superradiance $NC \gg 1$. Single-particle optical repumping proceeds at an optimum repumping rate $w \approx w_{\mathrm{pk}} = N\Gamma_c/2$ [1].

The ensemble of atoms can be represented by a Bloch vector $\vec{J}$ whose azimuthal phase $\phi(t)$ evolves in time at a rate set by $\dot{\phi}(t) = E(t)/\hbar$, where $E(t)$ is the instantaneous

*Author to whom correspondence should be addressed: bohnet@jilau1.colorado.edu

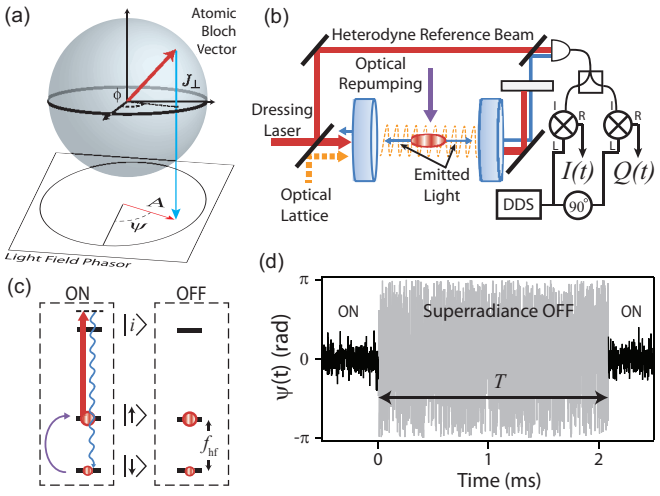

FIG. 1. (Color online) (a) Superradiant emission mapping the collective atomic coherence, represented by a Bloch vector $\vec{J}$ with phase ϕ and equatorial projection $J_\perp$, onto the phasor representing the emitted light field defined by a phase ψ and amplitude A. (b) The experimental setup. ^{87}Rb atoms are trapped in a 1D optical lattice (dashed, orange) within an optical cavity. Optical repumping light is applied perpendicular to the cavity axis. The emitted light is detected in heterodyne, then demodulated using a direct digital synthesis frequency reference to obtain both field quadratures $I(t)$ and $Q(t)$ and calculate the light's amplitude A and phase ψ. (c) An energy-level diagram of a superradiant Raman laser. The Raman dressing laser detuned from an intermediate state $|i\rangle$ induces optical decay at rate γ between ground hyperfine states $|\uparrow\rangle$ and $|\downarrow\rangle$. The atoms are incoherently repumped back to $|\uparrow\rangle$ at rate w. When the dressing and repumping lasers are off, the atoms remain in a superposition of $|\uparrow\rangle$ and $|\downarrow\rangle$, and the quantum phase $\phi(t)$ that evolves at $f_{\rm hf}$. (d) Example data from a Ramsey-like sequence in a superradiant laser. Superradiant emission continuously maps $\phi(t)$ onto $\psi(t)$. We measure a differential light phase $\psi(T) - \psi(0)$ over a free evolution time T.

energy difference separating $|\uparrow\rangle$ and $|\downarrow\rangle$, and $\hbar$ is the reduced Planck constant. Depending on the sensitivity of $E(t)$ to environmental conditions, precise measurements of $\phi(t)$ correspond to measurements of the environment or time [29].

The quantum phase $\phi(t)$ is not directly measurable and must be mapped onto an observable quantity. Bad-cavity active oscillators, such as masers or superradiant lasers, continuously map the collective phase $\phi(t)$ onto the observable phase $\psi(t)$ of an electromagnetic cavity field, because the rapidly decaying cavity field is slaved to the atomic coherence [13]. Ignoring vacuum noise, the complex electric field phasor is given by $A(t)e^{i\psi(t)} \propto J_\perp(t)e^{i\phi(t)}$, where $J_\perp(t)$ is the projection of the Bloch vector onto the x-y plane and $A(t)$ is the amplitude of the electric field phasor. Measuring the cavity field is equivalent to a continuous nondestructive measurement of the evolving atomic coherence.

The precision of the $\phi(t)$ to $\psi(t)$ mapping is limited by fundamental quantum noise from Schawlow-Townes phase diffusion of the atomic phase and photon shot noise on the measurement of the light phase. Measuring $\psi(t)$ longer reduces photon shot noise, but diffusion of the atomic phase means later data is less correlated with the initial atomic phase we wish to estimate. Employing a Kalman filter [30] analysis, we find that the optimal estimate $\phi_e(t)$ of the phase $\phi(t)$ is an exponentially weighted average of $\psi(t)$ with a weighting time constant

$$\tau_W = \frac{1}{\sqrt{q}N\Gamma_c}, \tag{1}$$

assuming $w = w_{\rm pk}$ (see Appendix A). Here q is the photon detection efficiency. A single-pole, low-pass filter can be used to implement such a running weighted average.

The mean-squared error of the optimal estimator is

$$\sigma_e^2 = \langle[\phi_e(t) - \phi(t)]^2\rangle = \frac{2}{\sqrt{q}N}. \tag{2}$$

When $q = 1$, the error is only a factor of 2 from the SQL on phase variance for a coherent spin state of N unentangled atoms $(\Delta\phi_{\rm SQL})^2 = 1/N$ and is at the SQL, $2(\Delta\phi_{\rm SQL})^2$, for the steady-state $J_\perp = \frac{N}{2\sqrt{2}}$ projection during superradiance at the optimum repumping rate $w_{\rm pk}$. Also, the impact of imperfect detection efficiency ($q < 1$) is mitigated by the scaling as $1/\sqrt{q}$ compared to the expected increase from increased photon shot noise alone, which would scale as $1/q$.

The measurement is nondestructive in that an atom experiences only $0.5/\sqrt{q}$ photon recoils on average during the characteristic measurement time τ_W. This degree of recoil heating compares favorably with other sample-preserving [31–34] and coherence-preserving [5,6,8,35] probing techniques with precision at the SQL.

This active superradiant mapping provides a continuous measurement of the atomic phase, in contrast to the standard technique for mapping a quantum phase onto the observable difference in state populations, as is done in passive Ramsey spectroscopy [36] with atomic fountain and optical lattice clocks, for example [37,38]. In Ramsey spectroscopy, the atoms accumulate a quantum phase $\phi(t)$ during free evolution periods after which $\phi(t)$ is mapped onto the atomic state populations. The state population is measured through fluorescence detection, which destroys the coherence and often destroys the ensemble [39], though the loss of the sample is not fundamental [31–34,40,41]. Passive Ramsey spectroscopy has the benefit of being free from perturbations necessarily introduced in the active mapping that disturb the accuracy of the measurement. By implementing dynamic control of the superradiant mapping, a passive Ramsey-like sequence can be realized in a superradiant laser, combining both active and passive sensing into a single hybrid system [14].

A single cycle of the hybrid sequence [Fig. 1(d)] consists of running steady-state superradiance and estimating the light phase $\bar{\psi}(0)$ just before temporarily shutting off the dressing and repumping lasers at time $t = 0$, quenching the superradiant emission. However, the collective Bloch vector continues to precess at frequency $f_{\rm hf}$ separating $|\uparrow\rangle$ and $|\downarrow\rangle$. At time $t = T$, the repumping and dressing lasers are turned on, and the phase of the light can then be estimated as $\bar{\psi}(T)$ using $\psi(t)$ data at times $t > T$. The accumulated atomic phase during the time period T is then $\Delta\phi(T) = \phi(T) - \phi(0) = \bar{\psi}(T) - \bar{\psi}(0)$. The variance on $\Delta\phi(T)$ is $2\sigma_e^2$ because of the measurement necessary to initialize the state at $T = 0$. The initial measurement is unnecessary in traditional Ramsey measurements with perfect state preparation.

The fundamental limit on the estimation of the phase difference $\Delta\phi(T)$ is a factor of 4 larger than for standard interferometry techniques that use traditional Ramsey spectroscopy at the SQL. Still, little fundamental precision needs to be sacrificed in future atomic sensors to utilize the proposed mapping. The collective nature of superradiant emission also results in a characteristic readout rate enhanced by a factor of N compared to the readout rate in the single-atom limit.

III. EXPERIMENTAL DEMONSTRATION

We have implemented a proof-of-principle atomic sensor using a cold-atom Raman laser on the clock transition of the ground hyperfine states of ^{87}Rb ($|\uparrow\rangle = |F = 2, m_F = 0\rangle$ to $|\downarrow\rangle = |F = 1, m_F = 0\rangle$). For our system, $\kappa/2\pi = 11$ MHz, $N = 10^6$ atoms cooled to 40 μK, $C = 8 \times 10^{-3}$, and $\gamma/2\pi \approx 1$ Hz. The cavity finesse is $F = 700$. The dressing and repumping lasers can be switched on and off within 100 ns, much faster than the time scale on which atomic dynamics occurs. We measure the phase $\psi(t)$ and amplitude $A(t)$ of the emitted light via heterodyne detection with respect to the dressing laser to remove phase noise on the emitted light imposed by phase noise on the dressing laser. By splitting the resulting rf signal and simultaneously demodulating the two quadratures, we obtain both $A(t)$ and $\psi(t)$ simultaneously. Example data of the passive sequence are shown in Fig. 1(d). We estimate $\phi(0)$ [$\phi(T)$] using linear fits to 0.5 ms of $\psi(t)$ data at times $t < 0$ ($t > T$).

The standard deviation of the light phase difference $\bar{\psi}(T) - \bar{\psi}(0)$ as $T \to 0$ predicted by the optimal estimator ϕ_e for our system is 12 ± 2 mrad, after accounting for finite quantum efficiency ($q = 0.03$) and the multilevel structure of ^{87}Rb. The general expression for the superradiant emission rate,

$$R_d = R\left(\frac{N}{2}\right)^2 \frac{2w}{N}\left(1 - \frac{w}{N\Gamma_c}\right), \tag{3}$$

accounts for $w \neq w_{\rm pk}$ and repumping through the multiple levels in the ^{87}Rb hyperfine structure [3] with the correction factor R. Here $N = 9 \times 10^5$ atoms, $\Gamma_c = 0.05$ s^{-1}, $R = 0.1$, and $w = 0.2NC\gamma$. The final result of $R \neq 1$ and $w \neq w_{\rm pk}$ is to reduce R_d by a factor of 0.28. The reduction in the emission rate and the subsequent modification to the phase diffusion increases σ_e by a factor of 2.4 compared to Eq. (2) (see Appendix A).

The observed standard deviation is 70 ± 7 mrad, a factor of 6 above the predicted noise. We assign the discrepancy to the dispersive tuning of the cavity mode described in Ref. [3], an effect present in our system, but not fundamental to the physics of the sensor. Building on this work, we have also demonstrated sensing of applied phase shifts using a superradiant magnetometer [14].

The analysis of the optimal estimator does not consider the impact of decoherence and dephasing in passive sensors with superradiant readout. The process of superradiant emission continually maintains the coherence of the ensemble, but when the emission is turned off, the atoms decohere, decreasing $J_\perp$ and A, as illustrated by Fig. 1(a). In addition to setting the fundamental resolution of the atomic phase, the coherence is vital to the reestablishment of superradiant emission after the evolution time, so the impact of decoherence must be understood for operation of future superradiant sensors.

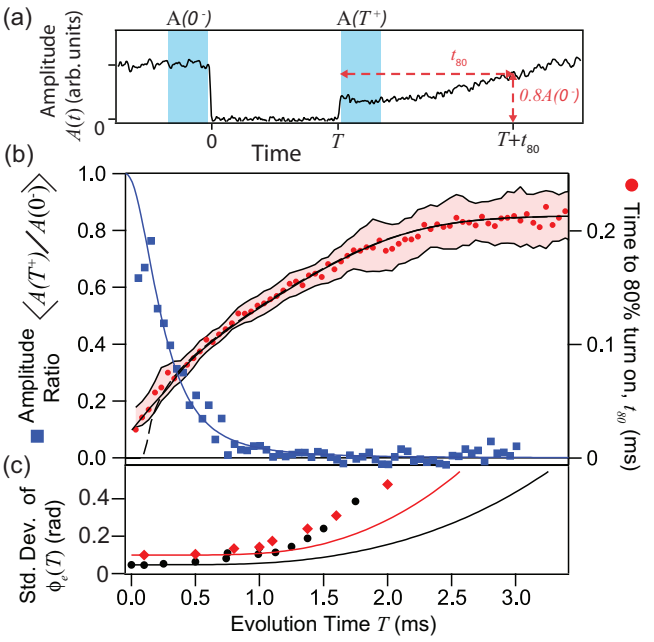

FIG. 2. (Color online) (a) Example time trace of the emitted light amplitude with an evolution time $T = 0.4$ ms. $A(0^-)$ and $A(T^+)$ are average amplitudes measured in the blue time windows before and after the evolution time. The characteristic rise time t_{80} is the time when the amplitude has returned to 80% of the steady-state value. (b) Left: The decay of $J_\perp$ as estimated by (blue squares) the ratio $A(T^+)/A(0^-)$ and (blue line) a fit to loss of contrast $c(t)$ of traditional Ramsey microwave spectroscopy. (b) Right: Measured (red circles) and predicted (line) recovery time t_{80}. The solid curve is the prediction accounting for the low-pass filter that was applied to the data. The band around the data indicates 1 standard deviation (s.d.) on each side of the data point. We attribute the fluctuations observed at short times to finite measurement precision. Each point is the average of 20 trials. (c) Standard deviation of the phase accumulated in time T as estimated by (diamonds) superradiant mapping and (circle) population mapping. The lines are predictions based on the observed loss of contrast $c(T)$.

We use the experimental sequence in Fig. 2(a) to study the decay of coherence. The amplitude of the emitted light field just before turn off, at $t = 0$, is $A(0^-)$ and just after turn on, at $t = T$, the amplitude is $A(T^+)$. When the evolution time T is short, the superradiance promptly returns to $A(0^-)$, but as the atomic coherence $J_\perp$ decays during the evolution time, $A(T^+)$ decreases proportionally. The decay of $J_\perp$ in our system is dominated by dephasing caused by inhomogeneous ac Stark shifts from the optical lattice. The ratio of amplitudes $A(T^+)/A(0^-)$ shown in Fig. 2(b) is well described by a fit to the decay of the contrast fringe $c(T)$ measured in standard microwave Ramsey spectroscopy with population readout [42].

The coherence lost during T is eventually restored as the laser returns to the steady state. In Fig. 2(b), the time t_{80} at which $A(T + t_{80})/A(0^-) = 0.8$ is compared to a theoretical prediction based on the observed atomic contrast $c(T)$. The prediction is obtained using semiclassical optical Bloch equations and is described in detail in Appendix B. At short

times, little coherence is lost, and the laser quickly returns to the steady state because the remaining coherence provides a seed for superradiance.

Ideally, superradiant readout should last long enough to completely restore the coherence and avoid depletion over multiple measurement cycles. We predict an average recovery time $t_{80} < \frac{2}{N\Gamma_C}$, which is confirmed by our experimental results in Fig. 2(b). Since the characteristic measurement time $\tau_W > \frac{1}{N\Gamma_C}$, each readout will almost fully restore the coherence for the next passive evolution measurement, as long as at least a small fraction of the coherence remains.

The collective atomic coherence $J_\perp(T)$ predominantly seeds subsequent superradiance until $J_\perp(T)$ becomes smaller than the rms equatorial projection of the decohered atoms $J_\perp^{(\mathrm{incoh})} \sim \sqrt{N}/2$. Even for $A(T^+)/A(0^-) \approx 0.05$, $J_\perp(T) > \sqrt{N}/2$, as seen by the relatively small t_{80} [Fig. 2(b)]. When $J_\perp(T) < J_\perp^{(\mathrm{incoh})}$, the laser must start an essentially new superradiant emission, resulting in large fluctuations in t_{80}. We observe fluctuations of 20 μs, on the same order as the predicted fluctuations in the time to reach the peak intensity of a superradiant pulse after preparation in the fully excited state [43].

We expect the fundamental phase resolution of the sensor to degrade from decoherence, because the signal, set by $J_\perp$, decays as $c(T)$, but the uncertainty from atom shot noise remains fixed. We predict the measurement noise by adding the background measurement noise in quadrature with the fundamental noise limit for both superradiant and population readout of a Ramsey sequence, $2\sigma_e/c(T)$ and $\sigma_e/c(T)$, respectively, shown as the lines in Fig. 2(c). Experimentally measuring the standard deviation of $\bar{\psi}(T) - \bar{\psi}(0)$ vs T, we see that even when $c(T)$ decays to $\approx$5% of the steady-state value at $T = 0.5$ ms, little phase resolution has been lost. The superradiant measurement noise at longer times is not at the decoherence limit due to additional technical noise, confirmed by the appearance of an equal amount of noise on the standard Ramsey population readout as well.

The culmination of these results is a demonstration of the nondestructive measurement technique in which we repeat on-off sequences to create a hybrid active-passive phase reference, shown in Fig. 3. The weight functions for the optimal estimate of the phase before and after the evolution periods are shown in Fig. 3(a). Each measurement both retains a large fraction of the atoms (>95%, with the loss believed to result primarily from light-assisted atomic collisions) and prepares the atomic coherence for future measurement cycles, as shown by the constant amplitude of the emission in Fig. 3(b). The free evolution times would ideally have high accuracy, while the active oscillation would have a much greater measurement bandwidth, providing the strengths of both active and passive phase references in a single device.

Furthermore, the duty cycle of the measurements could be adjusted in real time for optimal overall phase stability and accuracy given knowledge of the environment. Figures 3(a) and 3(b) show two example experimental trials where only the duty cycle has changed. Real-time adaptation might allow future hybrid phase references to be employed outside of the laboratory for both scientific and commercial applications [44].

IV. CONCLUSION

In some aspects, our technique is similar to recently demonstrated single-atom [32–34,40,41], sample-preserving [31], and nondemolition [5,6,8,35] readout techniques for neutral atoms where efficient collection of photons allows for detection near the SQL while in principle imparting only a few photon recoils per atom. Compared to fluorescence detection with a high numerical aperture lens, here the solid angle of the mode is small ($\Omega/4\pi = 8.9 \times 10^{-4}$), providing low backgrounds and high optical access.

However, our collective measurement is fundamentally different from the above techniques. Even nondemolition probes cause inevitable decay of the coherence that must be restored via discrete optical pumping and rotation of the state. In the superradiant readout, the active flow of collective information from the cavity also serves to reprepare the atomic coherence for the next measurement. The atomic phase continuously evolves across passive and active periods, allowing future frequency sources to be phase locked rather than frequency locked to an atomic reference, effectively eliminating aliasing noise in atomic clocks [45].

Looking forward, the ideas studied here might be applied on strictly forbidden optical atomic transitions [46], enabling hybrid optical lattice clocks suited for operation outside of carefully controlled laboratory environments. Though the system demonstrated in this work is of limited use for precision measurement, it nevertheless points a way forward to developing a different class of atomic sensors [14] and establishes the theoretical connection between fundamental laser linewidths and the information gained about the underlying system at the heart of the laser. Our work also highlights unique phenomena that emerge from collective coupling of many-body systems, a topic of much recent and future research, e.g., research with

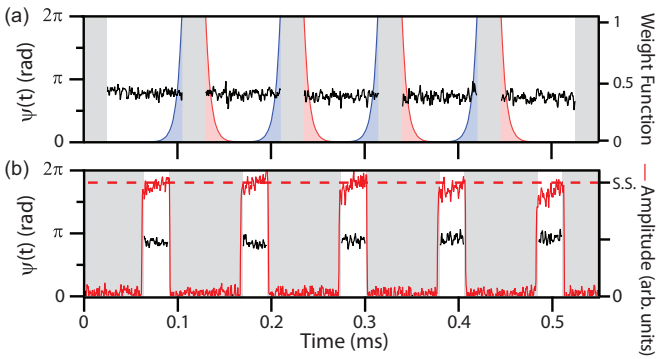

FIG. 3. (Color online) Demonstration of nondemolition superradiant measurements enabling a hybrid active-passive oscillator for two different duty cycles shown in (a) and (b). The measured light phase $\psi(t)$ is shown when the superradiance is switched on (black). The periods of evolution time, when the superradiance is switched off, are gray regions (random phase data not shown). The blue and red exponential curves in (a) correspond to the ideal optimal estimate weight functions before and after an evolution period, respectively, calculated with our experimental parameters of N, Γ_c, and q. (b) The emission amplitude (red) returns to the steady-state value (dashed line) during active oscillation, reflecting restoration of the coherence $J_\perp$.

quantum dots, superconducting qubits, ions, nitrogen-vacancy centers, and mechanical oscillators [47–51].

ACKNOWLEDGMENTS

We thank Jun Ye, Murray Holland, Dominic Meiser, and David Tieri for enlightening conversations. All authors acknowledge financial support from NSF PFC, NIST, ARO, and DARPA QuASAR. J.G.B. acknowledges support from NSF GRF, and Z.C. acknowledges support from A*STAR Singapore. This material is based upon work supported by the National Science Foundation under Grant No. 1125844.

APPENDIX A: DERIVATION OF OPTIMAL ESTIMATOR

Here we derive the optimal estimator $\phi_e(t)$ of the quantum phase $\phi(t)$, and its mean-squared error σ_e^2, given a measurement record $\psi(t)$ of the phase of the superradiantly emitted optical field. We use the results from a continuous Kalman filter analysis with uncorrelated process noise and measurement noise [30,52,53]. Here the measurement noise corresponds to the photon shot noise that appears in the measurement of the light phase $\psi(t)$ and the process noise corresponds to the phase diffusion of the collective atomic Bloch vector that sets the Schawlow-Townes frequency linewidth limit.

1. Photon shot noise

The measured phase of the radiated light is related to the underlying quantum phase $\phi(t)$ by $\psi(t) = \phi(t) + \Delta\psi(t)$, where the vacuum or photon shot noise adds the noise component $\Delta\psi(t)$. The noise is Poissonian and described by its lowest-order moments as $\langle\Delta\psi(t)\rangle = 0$ and $\langle\Delta\psi(t)\,\Delta\psi(t+\tau)\rangle = \delta(\tau)\Phi_m$. Here, $\delta(\tau)$ is the Dirac delta function so that the measurement noise at different times is uncorrelated, but when $\tau = 0$ it is equal to the constant $\Phi_m = \frac{1}{4R_d}$. $S_\phi^{(m)}(\omega)$ is the two-sided power spectral density (PSD) of phase fluctuations due to measurement noise, which for photon shot noise $S_\phi^{(m)}(\omega) = \int_{-\infty}^{\infty}\langle\Delta\psi(t)\,\Delta\psi(t+\tau)\rangle\cos(\omega t)dt = \Phi_m$ [54]. The light phase variance for a measurement time window Δt is $\sigma_m^2 = \int_{-\infty}^{\infty} S_\phi^{(m)}(\omega)|\frac{\mathrm{sinc}(\omega\Delta t/2)}{\sqrt{2\pi}}|^2 d\omega = \Phi_m/\Delta t = \frac{1}{4R_d\Delta t}$, where R_d is the average rate of detected superradiantly emitted photons using homodyne detection. At the optimum superradiant photon emission rate [1,3] $R_d = N^2\Gamma_c/8$, obtained at a repumping rate $w_{\mathrm{pk}} = N\Gamma_c/2$, where $\Gamma_c = \frac{C\gamma}{1+\delta^2}$ is the single-particle natural decay rate into the cavity mode, including a finite detuning of the cavity resonance frequency from the emission frequency δ in units of the cavity half linewidth $\kappa/2$. Taking into account finite quantum efficiency q, we find

$$S_\phi^{(m)}(\omega) = \frac{2}{qRN^2\Gamma_c}. \tag{A1}$$

2. Phase diffusion

In addition to measurement noise, the collective Bloch vector's quantum phase $\phi(t)$ diffuses with time as a result of quantum noise in the repumping process, the same mechanism that sets the Schawlow-Townes frequency linewidth limit in a bad-cavity laser or maser [1,26,27]. As a result, values of $\phi(t)$ at different times are less correlated with one another as the time separation grows. Specifically, the two-time phase difference (as measured in an appropriate rotating frame) averaged over many trials is zero, $\langle\phi(t+\tau) - \phi(t)\rangle = 0$, but the variance of the phase difference grows linearly with the time difference τ as

$$\sigma_D^2(\tau) = \langle[\phi(t+\tau) - \phi(t)]^2\rangle = D^2|\tau|. \tag{A2}$$

The phase diffusion coefficient D for the superradiant source can be derived from the expectation value of the two-time raising and lowering atomic operator $\langle\sigma_+(t+\tau)\sigma_-(t)\rangle$ in Ref. [55] and is

$$D^2 = \Gamma_c\left(1 + \frac{2w}{N\Gamma_c}\right). \tag{A3}$$

Assuming operation at the repumping rate w_{pk} one finds $D^2 = 2\Gamma_c$. For the Kalman filter analysis to follow, we utilize the PSD of frequency fluctuations defined as

$$S_f^{(p)}(\omega) = \int_{-\infty}^{\infty}\langle\dot\phi(t+\tau)\dot\phi(t)\rangle\cos(\omega\tau)d\tau \tag{A4}$$

for the process noise. From Eqs. (A2) and (A4), one simply finds $S_f^{(p)}(\omega) = D^2$.

3. Optimal phase estimation with Kalman filter

The Kalman filter [30,52,53] is designed to provide an optimal estimate $\phi_e(t)$ of the phase $\phi(t)$ that minimizes the mean-squared error in the estimate $\sigma_e^2 = \langle[\phi_e(t) - \phi(t)]^2\rangle$. The Kalman filter assumes the state model and noise sources are well known, and the that the process noise and measurement noise are uncorrelated, an assumption we verify by extending the theoretical work of Ref. [27] to the spectrum of phase fluctuations in a homodyne measurement.

For this simple case, the optimal Kalman filter takes the form of a single-pole low-pass filter. In the time domain, this is equivalent to an exponential weighting of the measurement record characterized by the exponential time constant τ_W. The time constant is the inverse of the Kalman gain K, which is calculated in steady state by a ratio of the noise power spectral densities

$$\tau_W = \frac{1}{K} = \left(\frac{S_\phi^{(m)}(\omega)}{S_f^{(p)}(\omega)}\right)^{1/2} = \frac{1}{\sqrt{q}N\Gamma_c}, \tag{A5}$$

assuming $w = w_{\mathrm{pk}}$. The optimal estimate is then the exponentially weighted average $\phi_e(t) = \frac{1}{\tau_W}\int_{-\infty}^{t}\psi(t')e^{-(t-t')/\tau_W}dt'$.

The mean-squared error in the optimal estimate is given by the geometric mean of the noise spectral densities

$$\sigma_e^2 = \left[S_f^{(p)}(\omega)S_\phi^{(m)}(\omega)\right]^{1/2} = \frac{2}{\sqrt{q}N}. \tag{A6}$$

Here we simply considered portions of the measurement record $\psi(t)$ at times $t \leqslant t_\circ$, as this is the only information actually available were the superradiance to be shut off at time $t_\circ$ as part of a Ramsey-like measurement. Conversely, an estimator of the phase just after superradiance is turned back on $\phi_e(t_\circ + T)$ will only include the measurement record at times $t \geqslant t_\circ + T$. The symmetry of the two noise processes with respect to time reversal makes it sufficient to consider only the first case.

4. Modifications for experimental conditions

To obtain a prediction for σ_e^2 observed here, we must also consider the modifications to $S_\phi^{(m)}(\omega)$ and $S_f^{(p)}(\omega)$ due to imperfections in our experiment. The general superradiant emission rate, Eq. (3), clearly modifies $S_\phi^{(m)}(\omega)$ in Eq. (A1). However, $S_f^{(p)}(\omega)$, given by the phase diffusion of the Schawlow-Townes limit, is also modified. As $S_f^{(p)}(\omega)$ corresponds to the full width at half maximum (FWHM) of the laser linewidth [55], we estimate the general form of the linewidth using Ref. [26],

$$\Delta f_{\mathrm{FWHM}} = \frac{1}{4\pi}\frac{w^2}{R_d} n_{\mathrm{inv}}, \tag{A7}$$

to calculate the modified $S_f^{(p)}(\omega)$. Here, $n_{\mathrm{inv}} = \frac{N_\uparrow}{N_\uparrow - N_\downarrow}$ is an inversion factor that depends on w and R through $N_\uparrow$ and $N_\downarrow$, the steady-state populations of $|\uparrow\rangle$ and $|\downarrow\rangle$, respectively. After simplification, $S_f^{(p)}(\omega)$ reduces to

$$S_f^{(p)}(\omega) = \Gamma_c \left(\frac{3}{2} + \frac{1}{R\left(\frac{N\Gamma_c}{w} - 1\right)} \right). \tag{A8}$$

APPENDIX B: PREDICTION OF TIME TO RETURN TO STEADY-STATE SUPERRADIANT EMISSION

To predict the time to restore the superradiant emission to steady state, characterized by t_{80} in the main text, we begin with a model based on semiclassical optical Bloch equations for the collective Bloch vector [55]. The cavity mode is adiabatically eliminated from the set of equations, justified by the cavity damping rate exceeding all other relevant rates in the system. We extend the model to include the full ground hyperfine structure of ^{87}Rb, which requires repumping lasers on both the $|F = 1\rangle \rightarrow |F' = 2\rangle$ transition and the $|F = 2\rangle \rightarrow |F' = 2\rangle$ transition to return atoms from $|\downarrow\rangle$ to $|\uparrow\rangle$. We also account for the Raman transition in our system by adiabatically eliminating the intermediate excited state and defining a two-photon atom cavity coupling g_2 as described in Ref. [3]. The model is similar to the cold-atom laser in Ref. [24], except that in this work, the cavity decay rate κ is much greater than the atomic coherence decay rate $\gamma_\perp \approx w/2$. Compared to the cold-atom lasers in Refs. [22,23], the atomic decoherence rate is much smaller here, because the atoms are confined in a far detuned optical lattice instead of a magneto-optical trap (MOT). Also, here the lasing occurs via a Raman transition between the magnetic-field-insensitive ground hyperfine states $|\uparrow\rangle = |F = 2, m_F = 0\rangle$ and $|\downarrow\rangle = |F = 1, m_F = 0\rangle$, as opposed to different Zeeman states.

To find the characteristic rise time $t_{80}(T)$ as a function of the evolution time T, we first solve the system of differential equations under steady-state conditions with the values of N, Γ_c, w, and R calculated from the measured shift of the cavity mode and laser powers in our experiment. We then assume that during the dark evolution time all populations remain at their original steady-state values, but that the collective coherence is reduced with respect to the original steady-state coherence $\bar{J}_\perp$ as $J_\perp(T) = c(T)\bar{J}_\perp$, where $c(T)$ is the fractional reduction in the Ramsey contrast fringe measured using traditional microwave spectroscopy and population readout shown in Fig. 3(b) in the main text. The loss of contrast $c(T)$ is consistent with dephasing caused by differential ac Stark shifts experienced by the trapped atoms [42]. To model the behavior once the coupling is restored at time T, we use the steady-state populations and modified coherence $J_\perp(T)$ as initial conditions to numerically integrate the equations and extract a predicted value of t_{80}.

[1] D. Meiser, J. Ye, D. R. Carlson, and M. J. Holland, Phys. Rev. Lett. **102**, 163601 (2009).
[2] J. Chen, Chin. Sci. Bull. **54**, 348 (2009).
[3] J. G. Bohnet, Z. Chen, J. M. Weiner, D. Meiser, M. J. Holland, and J. K. Thompson, Nature (London) **484**, 78 (2012).
[4] V. Meyer, M. A. Rowe, D. Kielpinski, C. A. Sackett, W. M. Itano, C. Monroe, and D. J. Wineland, Phys. Rev. Lett. **86**, 5870 (2001).
[5] J. Appel, P. Windpassinger, D. Oblak, U. Hoff, N. Kjærgaard, and E. Polzik, Proc. Natl. Acad. Sci. USA **106**, 10960 (2009).
[6] M. H. Schleier-Smith, I. D. Leroux, and V. Vuletić, Phys. Rev. Lett. **104**, 073604 (2010).
[7] I. D. Leroux, M. H. Schleier-Smith, and V. Vuletić, Phys. Rev. Lett. **104**, 073602 (2010).
[8] Z. Chen, J. G. Bohnet, S. R. Sankar, J. Dai, and J. K. Thompson, Phys. Rev. Lett. **106**, 133601 (2011).
[9] C. Gross, T. Zibold, E. Nicklas, J. Estève, and M. Oberthaler, Nature (London) **464**, 1165 (2010).
[10] M. Riedel, P. Böhi, Y. Li, T. Hänsch, A. Sinatra, and P. Treutlein, Nature (London) **464**, 1170 (2010).
[11] C. Deutsch, F. Ramirez-Martinez, C. Lacroûte, F. Reinhard, T. Schneider, J. N. Fuchs, F. Piéchon, F. Laloë, J. Reichel, and P. Rosenbusch, Phys. Rev. Lett. **105**, 020401 (2010).
[12] R. P. Feynman, F. L. Vernon, and R. W. Hellwarth, J. Appl. Phys. **28**, 49 (1957).
[13] J. G. Bohnet, Z. Chen, J. M. Weiner, K. C. Cox, and J. K. Thompson, Phys. Rev. Lett. **109**, 253602 (2012).
[14] J. M. Weiner, K. C. Cox, J. G. Bohnet, Z. Chen, and J. K. Thompson, Appl. Phys. Lett. **101**, 261107 (2012).
[15] L.-M. Duan, M. D. Lukin, J. I. Cirac, and P. Zoller, Nature (London) **414**, 413 (2001).
[16] A. D. Boozer, A. Boca, R. Miller, T. E. Northup, and H. J. Kimble, Phys. Rev. Lett. **98**, 193601 (2007).
[17] H. P. Specht, C. Nölleke, A. Reiserer, M. Uphoff, E. Figueroa, S. Ritter, and G. Rempe, Nature (London) **473**, 190 (2011).
[18] K. S. Choi, A. Goban, S. B. Papp, S. J. van Enk, and H. J. Kimble, Nature (London) **468**, 412 (2010).
[19] A. G. Radnaev, Y. O. Dudin, R. Zhao, H. H. Jen, S. D. Jenkins, A. Kuzmich, and T. A. B. Kennedy, Nat. Phys. **6**, 894 (2010).
[20] M. Lettner, M. Mücke, S. Riedl, C. Vo, C. Hahn, S. Baur, J. Bochmann, S. Ritter, S. Dürr, and G. Rempe, Phys. Rev. Lett. **106**, 210503 (2011).
[21] A. L. Schawlow and C. H. Townes, Phys. Rev. **112**, 1940 (1958).
[22] L. Hilico, C. Fabre, and E. Giacobino, Europhys. Lett. **18**, 685 (1992).

[23] W. Guerin, F. Michaud, and R. Kaiser, Phys. Rev. Lett. **101**, 093002 (2008).
[24] G. Vrijsen, O. Hosten, J. Lee, S. Bernon, and M. A. Kasevich, Phys. Rev. Lett. **107**, 063904 (2011).
[25] Q. Baudouin, N. Mercadier, V. Guarrera, W. Guerin, and R. Kaiser, Nat. Phys. **9**, 357 (2013).
[26] S. J. M. Kuppens, M. P. van Exter, and J. P. Woerdman, Phys. Rev. Lett. **72**, 3815 (1994).
[27] M. I. Kolobov, L. Davidovich, E. Giacobino, and C. Fabre, Phys. Rev. A **47**, 1431 (1993).
[28] H. Tanji-Suzuki, I. D. Leroux, M. H. Schleier-Smith, M. Cetina, A. T. Grier, J. Simon, and V. Vuletić, in *Advances in Atomic, Molecular, and Optical Physics*, edited by P. B. E. Arimondo and C. Lin (Academic, New York, 2011), Vol. 60, pp. 201–237.
[29] J. Kitching, S. Knappe, and E. A. Donley, IEEE Sens. J. **11**, 1749 (2011).
[30] R. E. Kalman and R. S. Bucy, J. Basic Eng. **83**, 95 (1961).
[31] J. Lodewyck, P. G. Westergaard, and P. Lemonde, Phys. Rev. A **79**, 061401 (2009).
[32] J. Bochmann, M. Mücke, C. Guhl, S. Ritter, G. Rempe, and D. L. Moehring, Phys. Rev. Lett. **104**, 203601 (2010).
[33] M. J. Gibbons, C. D. Hamley, C.-Y. Shih, and M. S. Chapman, Phys. Rev. Lett. **106**, 133002 (2011).
[34] A. Fuhrmanek, R. Bourgain, Y. R. P. Sortais, and A. Browaeys, Phys. Rev. Lett. **106**, 133003 (2011).
[35] Z. Chen, J. G. Bohnet, J. W. Weiner, K. C. Cox, and J. K. Thompson, arXiv:1211.0723.
[36] N. F. Ramsey, Phys. Rev. **78**, 695 (1950).
[37] S. Bize, P. Laurent, M. Abgrall, H. Marion, I. Maksimovic, L. Cacciapuoti, J. Grünert, C. Vian, F. P. dos Santos, P. Rosenbusch, P. Lemonde, G. Santarelli, P. Wolf, A. Clairon, A. Luiten, M. Tobar, and C. Salomon, J. Phys. B **38**, S449 (2005).
[38] A. D. Ludlow, T. Zelevinsky, G. K. Campbell, S. Blatt, M. M. Boyd, M. H. G. de Miranda, M. J. Martin, J. W. Thomsen, S. M. Foreman, J. Ye, M. Fortier, J. E. Stalnaker, S. A. Diddams, Y. Le Coq, Z. W. Barber, N. Poli, N. D. Lemke, K. M. Beck, and C. W. Oates, Science **319**, 1805 (2008).
[39] G. W. Biedermann, X. Wu, L. Deslauriers, K. Takase, and M. A. Kasevich, Opt. Lett. **34**, 347 (2009).
[40] R. Gehr, J. Volz, G. Dubois, T. Steinmetz, Y. Colombe, B. L. Lev, R. Long, J. Estève, and J. Reichel, Phys. Rev. Lett. **104**, 203602 (2010).
[41] J. Volz, R. Gehr, G. Dubois, J. Estève, and J. Reichel, Nature (London) **475**, 210 (2011).
[42] S. Kuhr, W. Alt, D. Schrader, I. Dotsenko, Y. Miroshnychenko, A. Rauschenbeutel, and D. Meschede, Phys. Rev. A **72**, 023406 (2005).
[43] M. Gross and S. Haroche, Phys. Rep. **93**, 301 (1982).
[44] D. R. Leibrandt, M. J. Thorpe, J. C. Bergquist, and T. Rosenband, Opt. Express **19**, 10278 (2011).
[45] P. Westergaard, J. Lodewyck, and P. Lemonde, IEEE Trans. Ultrason. Ferroelectr. Freq. Control **57**, 623 (2010).
[46] R. Santra, E. Arimondo, T. Ido, C. H. Greene, and J. Ye, Phys. Rev. Lett. **94**, 173002 (2005).
[47] M. Scheibner, T. Schmidt, L. Worschech, A. Forchel, G. Bacher, T. Passow, and D. Hommel, Nat. Phys. **3**, 106 (2007).
[48] J. M. Fink, R. Bianchetti, M. Baur, M. Göppl, L. Steffen, S. Filipp, P. J. Leek, A. Blais, and A. Wallraff, Phys. Rev. Lett. **103**, 083601 (2009).
[49] P. F. Herskind, A. Dantan, J. P. Marler, M. Albert, and M. Drewsen, Nat. Phys. **5**, 494 (2009).
[50] Y. Kubo, F. R. Ong, P. Bertet, D. Vion, V. Jacques, D. Zheng, A. Dréau, J.-F. Roch, A. Auffeves, F. Jelezko, J. Wrachtrup, M. F. Barthe, P. Bergonzo, and D. Esteve, Phys. Rev. Lett. **105**, 140502 (2010).
[51] A. Xuereb, C. Genes, and A. Dantan, Phys. Rev. Lett. **109**, 223601 (2012).
[52] R. E. Kalman, J. Basic Eng. **82**, 35 (1960).
[53] P. Zarchan and H. Musoff, *Fundamentals of Kalman Filtering: A Practical Approach* (AIAA, Reston, VA, 2001).
[54] J. Rutman, Proc. IEEE **66**, 1048 (1978).
[55] D. Meiser and M. J. Holland, Phys. Rev. A **81**, 033847 (2010).